Control of threshold enhancements in harmonic generation by atoms in a two-color laser field with orthogonal polarizations

M. V. Frolov,[1,2] N. L. Manakov,[1] T. S. Sarantseva,[2] A. A. Silaev,[2] N. V. Vvedenskii,[2] and Anthony F. Starace[3]

[1]*Department of Physics, Voronezh State University, Voronezh 394006, Russia*
[2]*Institute of Applied Physics, Russian Academy of Sciences, Nizhny Novgorod 603950, Russia*
[3]*Department of Physics and Astronomy, The University of Nebraska, Lincoln, Nebraska 68588-0299, USA*

Threshold phenomena (or channel-closing effects) are analyzed in high-order harmonic generation (HHG) by atoms in a two-color laser field with orthogonal linearly polarized components of a fundamental field and its second harmonic. We show that the threshold behavior of HHG rates for the case of a weak second harmonic component is sensitive to the parity of a closing multiphoton ionization channel and the spatial symmetry of the initial bound state of the target atom, while for the case of comparable intensities of both components, suppression of threshold phenomena is observed as the relative phase between the components of a two-color field varies. A quantum orbit analysis as well as phenomenological considerations in terms of Baz' theory of threshold phenomena [Zh. Eksp. Teor. Fiz. **33**, 923 (1957)] are presented in order to describe and explain the major features of threshold phenomena in HHG by a two-color field.

I. INTRODUCTION

High-order harmonic generation (HHG) is unique among strong laser field processes in having an extremely wide range of applications, including production of coherent XUV radiation [1,2] and attosecond pulses [3,4], monitoring of ultrafast phenomena on an attosecond time scale [5,6], and as a probe of atomic and molecular structures [7–9]. The HHG process is usually treated as a three-step process [10,11], since the HHG amplitude in the limit of low laser frequencies can be presented as a product of three factors associated with (i) tunnel ionization of a target atom or molecule, (ii) propagation of the ionized electron in the laser field, and (iii) its subsequent photorecombination on the ion of the parent atom with emission of a harmonic photon [12,13]. In this scenario, the recombination amplitude depends significantly on the electronic structure of the target atom or molecule, while the first two steps are governed mostly by the laser field. Obviously, variations of the temporal or spatial shape of a laser pulse crucially affects the first two steps of the three-step scenario. For example, changing the carrier envelope phase (CEP) of a linearly polarized short laser pulse drastically modifies the structure of the high energy part of the HHG spectrum [14,15], since the ionization and propagation steps are modified by variation of the CEP (cf. [16]). Using an elliptically polarized field in HHG experiments instead of a linearly polarized one makes possible the generation of elliptically polarized harmonics [13,17–19] and provides access to atomic characteristics (which are not available in HHG experiments with linearly polarized light) through measurement of the elliptical dichroism [20,21]. However, the disadvantage of an elliptically polarized field is that the HHG yield drops drastically with increasing ellipticity [13,17–19]. (For small ellipticity, this suppression can be approximated by a Gaussian function [22,23].)

A more promising HHG scheme for generation of intense XUV and attosecond pulses was suggested a decade ago [24–27] that involves a two-color pump field whose components are linearly polarized in orthogonal directions. If both components have comparable intensities, the yield of high-order harmonics can be enhanced and more intense attosecond pulses can be produced (as compared to a single frequency laser field) by adjusting the relative phase of the two components. As emphasized in Refs. [24–26], variation of the relative phase of the two components can affect the number of contributing classical electron trajectories in the quasiclassical description of the propagation step of the HHG process. The ability to select trajectories was demonstrated experimentally in Refs. [28,29]; see also the theoretical description of trajectory selection in Ref. [30] and the trajectory analysis in Ref. [31]. The two-color scheme with a fundamental and its weak second harmonic was proposed in Refs. [7,32–34] as a tool for probing atomic and molecular structure. The key idea is that a weak second harmonic component of a two-color field (steered by variation of the relative phase) can control the photoelectron recollision angle at the recombination stage. In this way, "angle-resolved" information about atomic or molecular orbits can be obtained from HHG spectra. In Ref. [35] it was demonstrated that by using this two-color scheme with a fundamental frequency in the midinfrared region one can enhance HHG by tuning the relative phase of the two components. A more spectacular application of the two-color scheme with orthogonal linearly polarized components was used to determine ionization and recombination times from an analysis of HHG spectra [5,36,37]. The two-color scheme was also proposed as a tool for HHG-based spectroscopy with the ability to retrieve both the angle-integrated photoionization cross section and the asymmetry parameter [38], which determines the angular distribution of photoelectrons [39].

Most theoretical analyses of HHG in a two-color field are based on a classical model, which assumes that during the propagation step the ionized electron moves in a laser field along closed classical (real) trajectories starting (after tunnel ionization) with zero velocity [10]. Such trajectories exist for a linearly polarized field [23], while for a two-dimensional field (including a two-color field) there are no trajectories that

satisfy such conditions. In this case, the interpretation of the numerical results is based on the real classical trajectories that "miss" the atomic ion (cf. [28–30,40,41]), i.e., the efficiency of recollision is estimated as the number of trajectories that return within an artificial sphere of radius r_0 about the ion. With increasing intensity of the second harmonic, the number of returning trajectories decreases, leading to the conclusion that the recombination step is suppressed. However, this interpretation has two drawbacks: (i) the number of returning trajectories depends crucially on the artificial parameter r_0; and (ii) the quantum recombination amplitude (which describes the efficiency of recombination) depends only on the atomic structure and is fairly independent of the parameter r_0. A more accurate analysis, based on quantum orbits [12,42], shows that the suppression of the HHG yield can be associated with suppression of the ionization step (cf. Ref. [23] for the case of an elliptically polarized field).

Besides the classical or quasiclassical features in HHG spectra, which can be quantitatively described in terms of classical trajectories, other features, such as threshold phenomena, have a purely quantum origin [43] and can lead to considerable resonancelike enhancements in HHG spectra. In order to describe these phenomena (or "channel closing" effects) quasiclassically, a huge number of complex quantum trajectories must be taken into account [44–46]. This fact shows the inapplicability of the standard quasiclassical approach, which is designed to treat only a few electron trajectories, and *a priori* manifests the quantum origin of channel closing effects. For the case of a monochromatic laser field, threshold phenomena in HHG have been extensively studied as a quantum effect in Refs. [43,47,48] and in terms of quantum orbits in Refs. [45,46]. Note that even for a short laser pulse these threshold phenomena occur in HHG spectra and depend crucially on the shape of the atomic potential [49–51]. However, for a two-color field with orthogonal linearly polarized components, threshold phenomena in HHG (and the possibility of their control by means of the relative phase of the two field components) have not yet been analyzed.

In this paper, we discuss threshold phenomena in HHG for a two-color field and their modifications with variation of the field parameters. This article is organized as follows. In Sec. II we discuss briefly some general definitions and models that we use in our analysis. Our numerical results are presented and discussed in Sec. III. To analyze our results, we use a classical closed trajectory treatment as well as more general quantum phenomenological considerations. In Sec. IV we summarize our results. Model analytic results for the HHG amplitude in a two-color field are presented in the Appendix. Atomic units are used throughout this article unless otherwise stated.

II. DEFINITIONS AND MODELS

We analyze threshold phenomena in a two-color field, whose electric field vector $\mathbf{F}(t)$ is parametrized as

$$\mathbf{F}(t) = F[\mathbf{e}_\omega \cos(\omega t) + \beta \mathbf{e}_{2\omega} \cos(2\omega t + \phi)], \qquad (1)$$

where F is the amplitude of the fundamental component with frequency ω, β describes the relative contribution of its second harmonic, ϕ is the relative phase between the two components, and their polarization vectors are denoted by $\mathbf{e}_\omega$ and $\mathbf{e}_{2\omega}$. Both

components are linearly polarized in orthogonal directions, so that the vectors $\mathbf{e}_\omega$ and $\mathbf{e}_{2\omega}$ are real and $(\mathbf{e}_\omega \cdot \mathbf{e}_{2\omega}) = 0$. For simplicity, we consider the vectors $\mathbf{e}_\omega$ and $\mathbf{e}_{2\omega}$ as directed along the X and Y axes, i.e., $\mathbf{e}_\omega = \hat{\mathbf{x}}$, $\mathbf{e}_{2\omega} = \hat{\mathbf{y}}$.

To describe the dynamics of an atomic system in a strong laser field, we employ two different atomic models. The first is based on the time-dependent effective range theory (TDER), which is appropriate for describing the nonperturbative strong-field dynamics of a weakly bound electron (e.g., as in a negative ion); it neglects long-range Coulomb effects [52,53]. The second model is based on the numerical solution of the time-dependent Schrödinger equation (TDSE), which helps in studying the threshold dynamics for a system with a Coulomb-type potential. We use these two models in order to show some general features of strong-field dynamics at the closing of a multiphoton detachment or ionization channel. In what follows, we briefly describe both the TDER model and the numerical algorithms for solving the TDSE.

A. Time-dependent effective range theory

The TDER model has been discussed in detail in Ref. [53] and its application to the description of the HHG process for both monochromatic and two-color fields has been presented in Refs. [38,54,55]. Thus we discuss here the general ideas of the TDER model and its application to the HHG process only briefly.

The TDER theory is based on the quasistationary quasienergy state (QQES) approach [56–59] and effective range theory [60]. The QQES approach is used for the quantum description of the laser-atom interaction, assuming the laser field is approximated by a periodic (in time) electric field. In the framework of the QQES approach the quantum state (QQES state) of an atomic electron in a periodic laser field is characterized by a complex quasienergy, whose real part gives the position of the atomic level (including the nonlinear Stark effect), while the imaginary part describes the total laser-induced width of the atomic level in the laser field [56–59]. The corresponding QQES wave function satisfies the complex boundary condition appropriate for an outgoing spherical wave at large distances, which ensures the complexity of the quasienergy. An advantage of the QQES approach is that it reduces the solution of the Cauchy problem for the TDSE to an eigenvalue problem, so that the complex quasienergy and QQES wave function can be found as the eigenvalue and its corresponding eigenfunction.

The dynamical part of the TDER model is based on effective range theory, i.e., the dynamical interaction of an active electron with an atomic core (which is modeled by a short-range potential) is described in terms of a single [52,53] or a few [61] scattering phases, which correspond to continuum channels with small orbital angular momenta l ($l = 0,1,2$). The TDER model assumes that there are two significantly different spatial regions: in the first region (at small distances), the atomic potential is important and the interaction of the active electron with the atomic core is described in terms of scattering phases [60], while at large distances (the second region) the atomic potential is negligible and all the dynamics is governed by the strong laser field. The wave functions from these two regions are matched by an appropriate boundary

condition [53,61], which is formulated at small distances. This matching reduces the four-dimensional eigenvalue problem to a one-dimensional integrodifferential equation for the complex quasienergy and QQES wave function at small distances [53].

As shown in Ref. [62], the complex quasienergy can be used to calculate the HHG amplitude. Indeed, according to Ref. [62], the HHG amplitude for a harmonic with frequency $\Omega = N\omega$ can be found as the derivative of the complex quasienergy in a two-color laser field comprised of a strong laser field and a weak (probe) harmonic field of frequency Ω. The advantage of the TDER model is that most of the calculations can be done analytically and the final results for the HHG amplitude can be presented in terms of one-dimensional integrals involving Bessel functions (see the Appendix). These integrals can be easily calculated numerically using the procedure suggested in Refs. [63,64]. This procedure transforms a one-dimensional integral to a form which is more convenient for numerical evaluation and theoretical analysis:

$$\int_0^\infty \frac{f(\tau)}{\sqrt{\tau}} e^{-i\alpha\tau} d\tau = \frac{1}{\sqrt{4\pi i}} \int_{-\infty}^\infty \frac{F(k)dk}{\sqrt{\alpha+k}},$$
$$F(k) = \int_{-\infty}^\infty f(\tau)e^{ik\tau} d\tau. \qquad (2)$$

Indeed, the Fourier transform, $F(k)$, of an analytic function $f(\tau)$ is a smooth function without branch points. Thus Eq. (2) shows explicitly that the result of integration over τ is a function having branch points in α. Since the function $f(\tau)$ is composed of trigonometric functions (see the Appendix), these branch points are located at the thresholds of multiphoton ionization channels, i.e., at $\alpha = N\omega$. Thus the TDER model is suitable for analyzing threshold phenomena for a short-range potential.

B. Numerical solution of the TDSE

To analyze threshold phenomena in a system with a Coulombic potential, we solve numerically the TDSE:

$$i\frac{\partial\psi}{\partial t} = -\frac{\nabla^2}{2}\psi + U(r)\psi + \mathbf{r}\cdot\mathbf{F}(t)f(t)\psi, \qquad (3)$$

where the function $f(t)$ describes the trapezoidal envelope of the laser pulse and $U(r)$ is the atomic potential. We use for $f(t)$ a trapezoidal envelope having a two-cycle ramp for turn on and off and a six-cycle flat top:

$$f(t) = \begin{cases} t/(2T), & 0 < t \leqslant 2T, \\ 1, & 2T < t \leqslant 8T, \\ 1-(t-8T)/(2T), & 8T < t \leqslant 10T, \\ 0, & t \leqslant 0, t > 10T, \end{cases}$$

where $T = 2\pi/\omega$. In order to avoid the Coulomb singularity at the origin, we employ an atomic potential having a smooth Coulomb potential (cf. Ref. [65]),

$$U(r) = -\alpha\,\mathrm{sech}^2(r/a) - \tanh(r/a)/r, \qquad (4)$$

with $a = 0.3$ and $\alpha = 2.17$. The values of a and α ensure that the energy of the ground state coincides with the H atom ground-state energy. The TDSE was solved by a split-step method with fast Fourier transform of the axes x, y, z [66]. The

temporal and spatial steps were chosen to ensure convergence of the numerical results: $\Delta t = 0.025$, $\Delta x = \Delta y = \Delta z = 0.3$. The number of grid nodes along each coordinate were $N_x = 512$, $N_y = N_z = 256$, and to suppress nonphysical reflections at the boundaries, absorption layers of width 15 a.u. were used. The HHG yield, $Y(\Omega)$, was calculated in terms of the Fourier transform of the dipole acceleration amplitude:

$$Y(\Omega) = \frac{|\mathbf{a}(\Omega)|^2}{2\pi c^3}, \quad \mathbf{a}(\Omega) = \int_{-\infty}^\infty e^{i\Omega t}\mathbf{a}(t)dt, \qquad (5)$$

where

$$\mathbf{a}(t) = -\mathbf{F}(t)f(t) - \langle\psi|\nabla U(r)|\psi\rangle. \qquad (6)$$

III. NUMERICAL RESULTS AND DISCUSSION

A. Numerical results

In Fig. 1 we present the dependence of the HHG rates [see Eqs. (A9) and (A12)] on the channel-closing number, R [51]:

$$R = (|E_0| + u_p)/\omega, \quad u_p = F^2/(4\omega^2)(1+\beta^2/4), \qquad (7)$$

where E_0 is the energy of the initial bound state. The channel-closing number increases with decreasing laser frequency ω and increasing laser intensity. Integer values of R, $R = k$, indicate the positions of k-photon ionization thresholds. In our calculations we vary only the intensity of the fundamental component and all other laser parameters, i.e., ω, β, and ϕ, are held fixed.

For the case of a weak second harmonic component, we present in Figs. 1(a) and 1(b) respectively the TDER results for odd and even HHG rates for an s state, while in Figs. 1(c) and 1(d) we present the corresponding TDER HHG rates for a p state. These numerical results are obtained using the analytic formulas for the TDER HHG amplitudes presented in the Appendix. For the s state, the rates of even and odd harmonics behave similarly: at the closing of an odd multiphoton ionization channel, the HHG rates show a smooth behavior, while at the thresholds of an even multiphoton ionization channel the HHG rates show "cusp" or "step"-like behavior. However, for the p-state, the cusp- or steplike behavior is observed at the thresholds of odd multiphoton ionization channels for odd harmonics and at the thresholds of even multiphoton ionization channels for even harmonics. These results show that for a weak second harmonic the threshold behaviors of HHG rates depend crucially on the orbital angular momentum of the electron in the initial state.

In order to show the collective behavior of HHG rates for a group of harmonics at the closing of a multiphoton ionization channel, in Figs. 2 and 3 we present the dependence of the integrated HHG yield on the channel-closing number for different values of ϕ and β. For the TDER results, the integrated HHG yield is defined as a sum over harmonic order n [48]:

$$P_{\Delta E} = \omega \sum_{n=n_i}^{n_f} n\mathcal{R}_n, \qquad (8)$$

where $\mathcal{R}_n$ is the HHG rate for the nth harmonic [see Eqs. (A9) and (A12)] and n_i and n_f are respectively the lower and upper harmonics involved. Since the HHG spectra are continuous
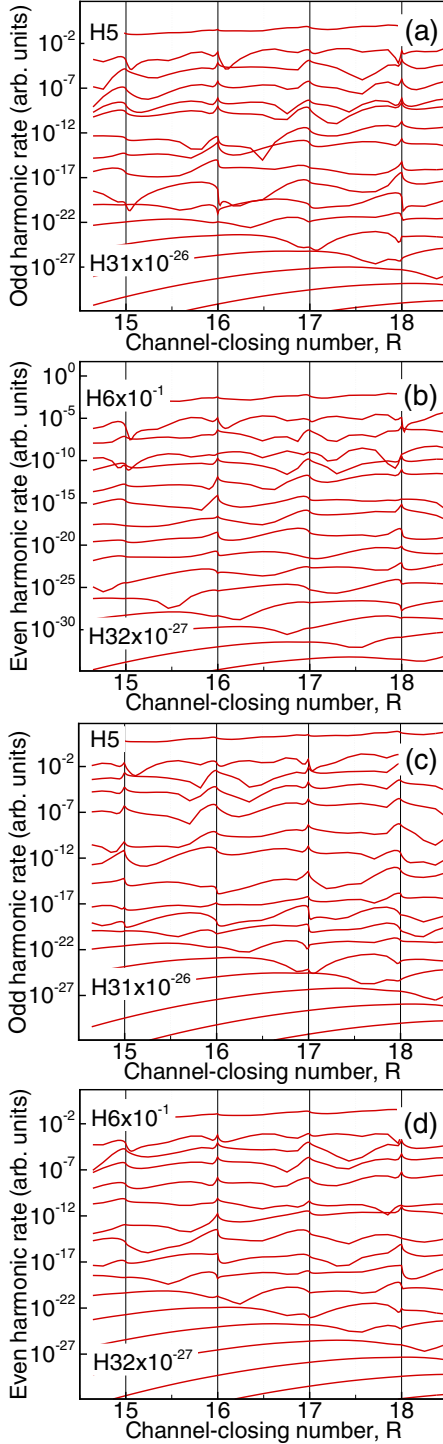
FIG. 1. Dependence of TDER model HHG rates on the channel-closing number R [see Eq. (7)] for varying intensity, $I = cF^2/(8\pi)$, and fixed wavelength, $\lambda = 800$ nm, of the fundamental field, $\beta = 0.2$, and relative phase $\phi = 0$. The intensity I is changed in the range $1.3 \times 10^{14} \leq I \leq 2.2 \times 10^{14}$ W/cm². For easier comparison, each curve is multiplied by a factor $10^{-(N-5)}$, where N is the harmonic number. N is odd for (a) and (c) and even for (b) and (d). Panels (a) and (b): results for a bound s state; panels (c) and (d): results for a bound p state. The binding energy is $|E_0| = 15.76$ eV, as for the argon atom.

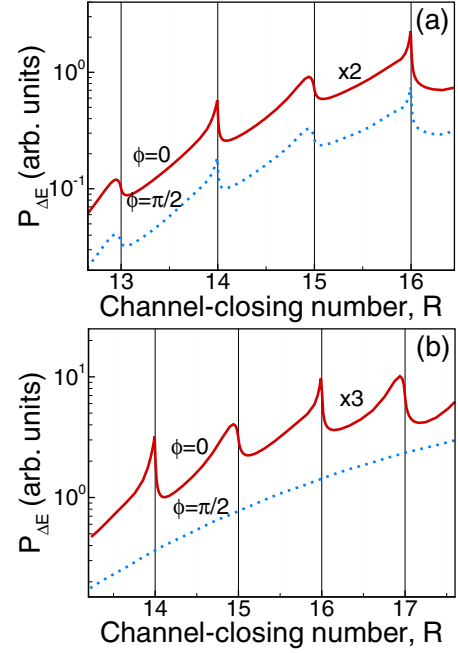FIG. 2. Integrated TDER model HHG yields $P_{\Delta E}$ (8) for an initial s state ($|E_0| = 15.76$ eV) and a harmonic energy range $\Delta E = (20–50)$ eV for the laser field (1) as a function of the channel-closing number R (7). The fundamental field component has a wavelength $\lambda = 800$ nm and an intensity I that varies over the range $1.3 \times 10^{14} \leq I \leq 2.2 \times 10^{14}$ W/cm². Solid (red) lines: $\phi = 0$; dotted (blue) lines: $\phi = \pi/2$. Panel (a): $\beta = 0.2$; panel (b): $\beta = 0.8$.

in TDSE calculations for a short pulse, we define in this case the integrated yield as an integral over harmonic energy [49–51,67]:

$$P_{\Delta E} = \frac{1}{\mathcal{T}} \int_{E_i}^{E_f} Y(\Omega) d\Omega, \qquad (9)$$

where $Y(\Omega)$ is the HHG yield [see Eq. (5)], $\mathcal{T}$ is the duration of the laser pulse, and E_i and E_f are respectively the lower and upper energy limits of the harmonics involved. In our TDSE calculations the lower and upper limits for the harmonic energy are $n_i \hbar\omega \approx E_i = 20$ eV and $n_f \hbar\omega \approx E_f = 50$ eV, respectively.

We present in Fig. 2 the TDER results for a bound s state with $|E_0| = 15.76$ eV and in Fig. 3 the TDSE results for the H atom ground state. For a weak second harmonic [see Figs. 2(a) and 3(a)], the threshold phenomena are almost independent of the relative phase ϕ. For a short-range potential, sharp cusps are shown at the closing of even multiphoton ionization channels and more smooth behaviors occur at the thresholds of odd channels (cf. Ref. [48]). However, for the Coulombic potential, the threshold peaks for both odd and even ionization thresholds are similar and are shifted by about half the photon energy, $\hbar\omega/2$, similar to the shifts in Refs. [49–51] for a monochromatic field. With increasing intensity of the second harmonic [see Figs. 2(b) and 3(b)], the threshold behavior of $P_{\Delta E}$ becomes sensitive to the relative phase ϕ. Indeed, for $\phi = 0$, the dependence of $P_{\Delta E}$ on R looks similar
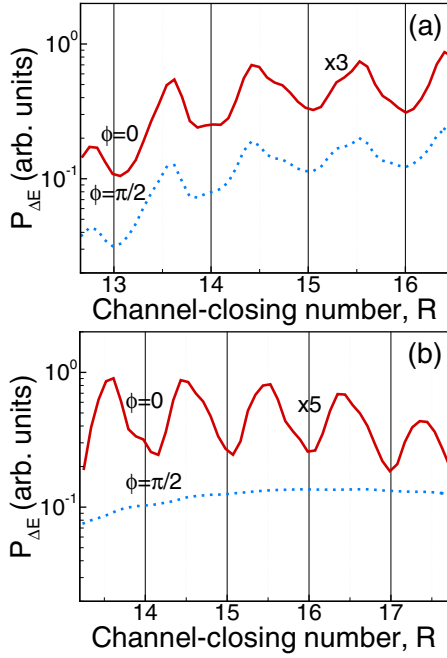
FIG. 3. TDSE results for the integrated HHG yield $P_{\Delta E}$ (9) for the H atom ground state for the same laser parameters as in Fig. 2.

to that for the case of a weak second harmonic. However, threshold singularities in the R dependence of $P_{\Delta E}$ completely disappear for $\phi = \pi/2$. In order to describe the aforementioned threshold features of HHG spectra in a two-color field, we present in Sec. III B a trajectory analysis and in Sec. III C a phenomenological quantum mechanical analysis.

B. Trajectory analysis

The commonly accepted method for analysis of HHG spectra in the low frequency limit is based on the evaluation of the temporal integrals in the HHG amplitude by the method of steepest descent [12]. Within this approach, the HHG amplitude can be presented as a sum of partial amplitudes associated with a closed quantum trajectory (or "quantum orbit") that starts at the time t_i and ends at the time t_f. These quantum trajectories satisfy Newton's equation and in general the times t_i and t_f are complex. The system of equations for the times t_i and t_f is found from the adiabaticity condition for electron transitions between initial and final states at those two times [12], i.e., at the "moment" of transition, the energies of the initial and final states should be equal [60]:

$$E(t_i, \mathbf{k}) = E_0, \tag{10a}$$

$$E(t_f, \mathbf{k}) = E, \quad E = \Omega + E_0, \tag{10b}$$

where

$$E(t; \mathbf{k}) = \tfrac{1}{2}(\mathbf{k} + \mathbf{A}(t)/c)^2, \tag{11}$$

$$\mathbf{k} \equiv \mathbf{k}(t_i, t_f) = -\frac{1}{c(t_f - t_i)} \int_{t_i}^{t_f} \mathbf{A}(\tau) d\tau, \tag{12}$$

and $\mathbf{A}(t)$ is the vector potential of the electric field $\mathbf{F}(t)$ in Eq. (1). Equation (10a) corresponds to the transition from

an initial state with (negative) energy E_0 to the laser-dressed continuum state with energy $E(t_i, t_f)$ at time t_i, while Eq. (10b) corresponds to the transition from the laser-dressed continuum state to the initial state with emission of a harmonic photon with energy Ω. The form of $\mathbf{k}$ in Eq. (12) ensures that the contributing orbits are closed trajectories [12].

In the classical model of HHG, the energy E_0 in Eq. (10a) is replaced by zero, indicating that the active electron is liberated from the atom to the continuum with zero initial kinetic energy. For the case of linear polarization, the system of equations (10) has *real* solutions for $E_0 \to 0$, while for a two-color field with perpendicular linearly polarized components there are no *real* solutions, even in the classical limit. The times given by the classical model play a crucial role in the analysis of the HHG amplitude, since only those quantum trajectories whose times are close to the classical ones contribute significantly to the HHG amplitude because the corresponding classical actions for these quantum paths have the smallest imaginary parts [60,68]. Thus we shall analyze the solutions of the system (10) for a two-color field (1) paying special attention to their closeness to the classical solutions for a linearly polarized field.

1. Case of a weak second harmonic component

For the case of a weak second harmonic in the field (1), we represent the system of equations (10) in the explicit form:

$$\sin \tau_i + \frac{\cos \tau_f - \cos \tau_i}{\tau_f - \tau_i} = \pm i\Gamma, \tag{13a}$$

$$\sin \tau_f + \frac{\cos \tau_f - \cos \tau_i}{\tau_f - \tau_i} = \mp(\sqrt{\epsilon} - \Lambda), \tag{13b}$$

where

$$\Gamma \equiv \Gamma(\tau_i, \tau_f) = \sqrt{\gamma^2 + \epsilon_y(\tau_i)}, \tag{14}$$

$$\Lambda \equiv \Lambda(\tau_i, \tau_f) = \frac{\epsilon_y(\tau_f)}{\sqrt{\epsilon - \epsilon_y(\tau_f)} + \sqrt{\epsilon}}, \tag{15}$$

$$\epsilon_y(\tau) = [A_y(\omega^{-1}\tau)/c + k_y]^2/(2u_p)$$
$$= \frac{\beta^2}{4}\left[\sin(2\tau + \phi) + \frac{\cos(2\tau_f + \phi) - \cos(2\tau_i + \phi)}{2(\tau_f - \tau_i)}\right]^2, \tag{16}$$

$\gamma = \omega\sqrt{2|E_0|}/F$, $\tau_i = \omega t_i$, $\tau_f = \omega t_f$, and $\epsilon = E/(2u_p)$. Since $\gamma \ll 1$ and $\beta \ll 1$ ($\epsilon_y \propto \beta^2 \ll 1$), both Γ and Λ are less than unity and can be treated as perturbations in the system of equations (13). Note that for $\epsilon > \epsilon_y(\tau_f)$ (above-threshold harmonics) Λ is real, for $0 < \epsilon < \epsilon_y(\tau_f)$ (near-threshold harmonics) it is complex, and for $\epsilon < 0$ (below-threshold harmonics) Λ has only an imaginary part. In our analysis we consider only above-threshold harmonics, since the near- and below-threshold harmonics require a separate treatment.

To zero order in β, the times τ_i and τ_f are approximated by the *real* classical times $\tau_i^{(cl)}$ and $\tau_f^{(cl)}$ for a linearly polarized

field, which can be found from the system of equations:

$$\sin \tau_i^{(cl)} + \frac{\cos\left(\tau_f^{(cl)}\right) - \cos(\tau_i^{(cl)})}{\tau_f^{(cl)} - \tau_i^{(cl)}} = 0, \tag{17a}$$

$$\sin \tau_f^{(cl)} + \frac{\cos(\tau_f^{(cl)}) - \cos\left(\tau_i^{(cl)}\right)}{\tau_f^{(cl)} - \tau_i^{(cl)}} = \sqrt{\epsilon}. \tag{17b}$$

The correction to the classical times can be found by presenting τ_i and τ_f in the form $\tau_i = \tau_i^{(cl)} + \Delta_i$, $\tau_f = \tau_f^{(cl)} + \Delta_f$ and expanding the left-hand side of the system of equations (13) in power series in Δ_i and Δ_f. In the first order of perturbation theory, Δ_i and Δ_f can be found in the form:

$$\Delta_i = \frac{\sqrt{\epsilon}\, \Lambda\left(\tau_i^{(cl)}, \tau_f^{(cl)}\right)}{\left|\cos\left(\tau_i^{(cl)}\right)\right|\left(\sqrt{\epsilon} - \Delta\tau^{(cl)}\left|\cos \tau_f^{(cl)}\right|\right)} + i\frac{\Gamma\left(\tau_i^{(cl)}, \tau_f^{(cl)}\right)}{\left|\cos\left(\tau_i^{(cl)}\right)\right|}, \tag{18a}$$

$$\Delta_f = \frac{\Lambda\left(\tau_i^{(cl)}, \tau_f^{(cl)}\right)}{\sqrt{\epsilon}/\Delta\tau^{(cl)} - \left|\cos \tau_f^{(cl)}\right|}. \tag{18b}$$

Equations (18) show that the nonzero second harmonic component leads to *real* shifts of the times τ_i and τ_f from the classical ionization and recombination times $\tau_i^{(cl)}$ and $\tau_f^{(cl)}$, while for $\beta = 0$ these shifts vanish. The second harmonic component of a two-color field also increases the imaginary part of the ionization time and makes it ϕ dependent, thereby introducing a ϕ dependence in the ionization step of the three-step HHG scenario:

$$\text{Im} \int_{t_i}^{t_f} \left\{ \frac{1}{2}\left[\frac{1}{c}\mathbf{A}(t) + \mathbf{k}\right]^2 - E_0 \right\} dt \approx -\frac{4u_p \Gamma^3\left(\tau_i^{(cl)}, \tau_f^{(cl)}\right)}{3\omega|\cos\left(\tau_i^{(cl)}\right)|}. \tag{19}$$

Since $\beta \ll 1$ and on each half-period of the fundamental field ionization occurs at the maximum of the laser field, while recombination takes place at a zero of the field, we can approximate $\tau_i^{(cl)} \approx \pi m$ and $\tau_f^{(cl)} \approx \tau_i^{(cl)} + \pi/2 + \pi k$ with integer m and k. Within this approximation, the result (16) for $\epsilon_y(\tau_i^{(cl)})$ can be estimated as follows:

$$\epsilon_y\left(\tau_i^{(cl)}\right) \approx \frac{\beta^2}{4}\sin^2 \phi. \tag{20}$$

Therefore, the ionization step is more suppressed for $\phi = \pi/2$ than for $\phi = 0$ and thus the HHG yield is larger for $\phi = 0$ than for $\phi = \pi/2$. Our analysis above shows that adding a weak second harmonic component slightly perturbs the ionization and recombination times for quantum trajectories compared to the case of a linearly polarized single-component field. These times are still close to the classical times for linear polarization. Therefore, in the two-color field with a weak second harmonic component, the phenomena originating from the interference of many quantum orbits (such as threshold phenomena [45,46]) should be observed as for the case of a single-component linearly polarized laser field.

2. Case of comparable intensities of the two components

Since the contribution of the term $\epsilon_y(\tau)$ in the system of equations (13) cannot be considered perturbatively in the case

of comparable intensities of the two components of a two-color field, for analysis of the system of equations (10) for this case we apply a different method. First, we consider the classical limit of the system of equations (10). According to the classical model, the energy of the electron at the time $t = t_i^{(cl)}$ equals zero, so that both x and y components of the electron momentum reduce to zero at the time $t = t_i^{(cl)}$, i.e.,

$$A_j\left(t_i^{(cl)}\right)/c + k_j^{(cl)} = 0, \quad j = x,y,$$
$$\mathbf{k}^{(cl)} = \mathbf{k}\left(t_i = t_i^{(cl)}, t_f = t_f^{(cl)}\right). \tag{21}$$

The system of equations (21) can be rewritten explicitly in the form

$$\sin \tau_i^{(cl)} + \frac{\cos\left(\tau_f^{(cl)}\right) - \cos\left(\tau_i^{(cl)}\right)}{\tau_f^{(cl)} - \tau_i^{(cl)}} = 0, \tag{22a}$$

$$\sin\left(2\tau_i^{(cl)} + \phi\right) + \frac{\cos\left(2\tau_f^{(cl)} + \phi\right) - \cos\left(2\tau_i^{(cl)} + \phi\right)}{2\left(\tau_f^{(cl)} - \tau_i^{(cl)}\right)} = 0. \tag{22b}$$

The coupled system of equations (22) cannot be solved for real times. Nevertheless, we shall analyze separately the solution of each equation in the system (22) in terms of real-valued functions $\tau_i^{(cl)} = \tau_i^{(cl)}(\tau_f^{(cl)})$.

For large $\Delta\tau^{(cl)} = \tau_f^{(cl)} - \tau_i^{(cl)}$, the solutions of Eqs. (22a) and (22b) can be given as a series in $[\Delta\tau^{(cl)}]^{-1}$:

$$\tau_i^{(cl)} \approx a_0 + \frac{a_1\left(\tau_f^{(cl)}\right)}{\Delta\tau^{(cl)}} + \frac{a_2\left(\tau_f^{(cl)}\right)}{[\Delta\tau^{(cl)}]^2} + \cdots. \tag{23}$$

Substituting Eq. (23) into the system of equations (22) with subsequent expansions of the left-hand sides in series in $[\Delta\tau^{(cl)}]^{-1}$, we obtain sequentially from Eqs. (22a) and (22b) the solutions to first order in $[\Delta\tau^{(cl)}]^{-1}$:

$$\tau_i^{(cl)} \approx -\pi n_1 - (-1)^{n_1}\frac{\cos \tau_f^{(cl)} - (-1)^{n_1}}{\tau_f^{(cl)} + \pi n_1}, \tag{24a}$$

$$\tau_i^{(cl)} \approx -\frac{\pi n_2}{2} - \frac{\phi}{2} - (-1)^{n_2}\frac{\cos\left(2\tau_f^{(cl)} + \phi\right) - (-1)^{n_2}}{2\left(2\tau_f^{(cl)} + \pi n_2\right)}, \tag{24b}$$

where n_1 and n_2 are positive integers. The asymptotic solutions (24a) and (24b) show explicitly that both solutions merge for large n_1 and n_2 if $n_2 = 2n_1$ and $\phi = 0$ [see Fig. 4(a)], while for $\phi = \pi/2$ and large n_1 and n_2 they never cross [see Fig. 4(b)]. It should be noted that for $\phi = 0$ the system of equations (22) has "trivial" solutions [31]: $\tau_f^{(cl)} = 0, \pi, 2\pi$, $\tau_i^{(cl)} = \tau_f^{(cl)} - 2\pi n$, where n is a positive integer. For odd n_1 and $n_2 = 2n_1$, the solution (24a) coincides exactly with the solution (24b) at $\phi = 0$ and $\tau_f^{(cl)} = \pi$, and, for even n_1 and $n_2 = 2n_1$, at $\phi = 0$, $\tau_f^{(cl)} = 0$, and $\tau_f^{(cl)} = 2\pi$ [see Fig. 4(a)].

For a small difference $\tau_f^{(cl)} - \tau_i^{(cl)}$ (or small $\Delta\tau^{(cl)}$), solutions of (22) can be given as series in $\Delta\tau^{(cl)}$. Indeed,
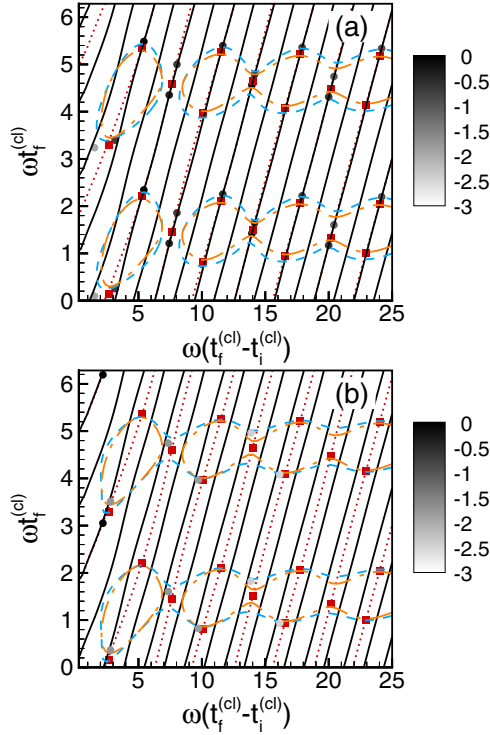
FIG. 4. Solutions of Eqs. (10) and (22) for two relative phases of the two-color laser field components: (a) $\phi = 0$; (b) $\phi = \pi/2$. *Dotted (red) lines*: solutions of Eq. (22a); *solid (black) lines*: solutions of Eq. (22b); *dot-dashed (orange) lines*: solutions of Eq. (10b) for $\beta = 0$; *dashed (blue) lines*: solutions of Eq. (10b) for $\beta \neq 0$; *solid circles*: exact solutions of the system (10), with the real parts of the times t_i and t_f used for plotting and with the intensity of the circle shading indicating the relative contribution (on a logarithmic scale) of the corresponding saddle points to the partial HHG amplitudes, with black indicating the strongest contribution and light gray the least. *Solid (red) squares*: exact solutions of the system of equations (10) for $\beta = 0$, with the real parts of the times t_i and t_f used for plotting. Calculations have been carried out for $I = cF^2/(8\pi) = 2 \times 10^{14}$ W/cm^2, $\beta = 0.8$ [except for the dot-dashed (orange) lines and the solid (red) squares], $\lambda = 800$ nm, $|E_0| = 13.65$ eV, and $E = 1.7u_p \approx 20.32$ eV.

substituting in (22a) the times $\tau_i^{(\text{cl})}$ and $\tau_f^{(\text{cl})}$ in the form

$$\tau_i^{(\text{cl})} = \tau_f^{(\text{cl})} - \Delta\tau^{(\text{cl})}, \quad \tau_f^{(\text{cl})} = \sum_j b_j [\Delta\tau^{(\text{cl})}]^j \quad (25)$$

and then expanding (22a) in a series in $\Delta\tau^{(\text{cl})}$ and equating coefficients of the term $[\Delta\tau^{(\text{cl})}]^j$, we obtain a coupled system of equations for the coefficients b_j. The values of the first few b_j are given by

$$b_1 = \frac{1}{3}, \quad b_3 = -\frac{1}{810}, \quad b_5 = -\frac{1}{68040}, \quad b_7 = -\frac{1}{6123600},$$

$$b_0 = \frac{\pi}{2} + \pi n, \quad b_{2k} \equiv 0, \quad n = 0,1, \quad k = 1,2,\ldots. \quad (26)$$

The series in Eq. (25) is rapidly convergent: e.g., for $\Delta\tau^{(\text{cl})} = \pi$, the term $b_7[\Delta\tau^{(\text{cl})}]^7 \approx 5 \times 10^{-4}$ and thus the expansion (25) can be used even for $\Delta\tau^{(\text{cl})} \sim \pi$. The solution of Eq. (22b) can be obtained from the expansion (25), substituting there $\tau_f^{(\text{cl})} \rightarrow$

$(2\tau_f^{(\text{cl})} + \phi)$ and $\Delta\tau^{(\text{cl})} \rightarrow 2\Delta\tau^{(\text{cl})}$. By taking into account three terms in the expansion of $\tau^{(\text{cl})}$, we obtain from Eq. (22a):

$$\tau_f^{(\text{cl})} \approx \frac{\pi}{2} + \pi k + \frac{\Delta\tau^{(\text{cl})}}{3} - \frac{[\Delta\tau^{(\text{cl})}]^3}{810}, \quad (27)$$

while from Eq. (22b) we have

$$\tau_f^{(\text{cl})} \approx \frac{\pi}{4} + \frac{\pi n}{2} - \frac{\phi}{2} + \frac{\Delta\tau^{(\text{cl})}}{3} - \frac{2[\Delta\tau^{(\text{cl})}]^3}{405}, \quad (28)$$

where $k = 1,2$ and $n = 1,2,3,4$. For $\phi = \pi/2$ and even n these solutions merge as $\Delta\tau^{(\text{cl})} \rightarrow 0$. Owing to the smallness of b_j, the difference of the results (27) and (28) for $\phi = \pi/2$ is observable only at $\Delta\tau^{(\text{cl})} \sim \pi$ (see Fig. 4).

Since the solutions of Eq. (10b) for positive energy E (i.e., for harmonics in the plateau region) can be found for real times for any phase ϕ and any intensity of the laser field components (see Fig. 4), they cross the solutions of the system of equations (22), whose asymptotic behavior is discussed above. The crossing points of the solutions of Eq. (10b) with the solutions of Eqs. (22a) and (22b) are closest when the solutions of Eqs. (22a) and (22b) are close to each other. According to our analysis above for $\phi = 0$, at such close crossing points we use the crossing point with the solutions of Eq. (22a) [see Fig. 4(a)], while for $\phi = \pi/2$ close crossing points occur only for small $\Delta\tau^{(\text{cl})}$ [see Fig. 4(b)]. The dominant contributions to the HHG amplitude saddle points from Eq. (10) are near the close crossing points. The contributions of these saddle points are much stronger than are those of others since such trajectories are much closer to the classical ones. Indeed, in Fig. 4 we present the exact solutions of the system of equations (10) (real parts of t_f and t_i are presented) and their relative contributions to the HHG amplitude, which are marked by the density of shading (with the saddle points that contribute most shown in black, while those contributing less are in light gray). The position of the saddle points is guided by the close crossing points and, as we see from Fig. 4, for $\phi = 0$ the number of contributing points is quite large. They occur near the saddle points for the monochromatic field case and thus the corresponding trajectory-interference effects should be well pronounced, as for the case of a linearly polarized monochromatic field. Since for $\phi = \pi/2$ there is only a single contributing saddle point on each half-period of the laser field, the interference effects in HHG spectra originating from the interference between the partial HHG amplitudes are suppressed. According to the quasiclassical picture of threshold phenomena [45,46], these phenomena originate from in-phase or out of phase interference of a large number of quantum trajectories. As shown by the above analysis, for the case of a two-color field, the number of contributing trajectories can be controlled by changing the phase ϕ from 0 to $\pi/2$, which gradually reduces the number of interfering trajectories with increasing ϕ and thus gradually reduces the manifestation of threshold phenomena. This consideration explains the suppression of threshold phenomena in Figs. 2 and 3 for comparable intensities of the fundamental and second harmonic components of the two-color field for a relative phase $\phi = \pi/2$. We emphasize that this explanation of the significant dependence of threshold phenomena on the relative phase of the two-color field is valid for both short-range and

Coulomb-like potentials, despite the fact that the shapes of the threshold phenomena for these two potentials for $\phi = 0$ [cf. Figs. 2(b) and 3(b)] differ significantly.

C. Quantum analysis of threshold phenomena in the two-color field

The quantum orbit approach allows one to analyze how the number of electron trajectories contributing to the HHG amplitude depends on the intensities and relative phase of a two-color laser field. However, this approach is inappropriate for analyzing HHG rates near the thresholds of multiphoton ionization channels since near these thresholds a very large number of partial HHG amplitudes (associated with corresponding quantum orbits) contribute [45,46]. The constructive or destructive interference of partial amplitudes is governed by the phases of these amplitudes, which are difficult to calculate analytically for a strong monochromatic laser field [45]. Such calculations become even more complicated for the case of a two-color field. In particular, this drawback of a quantum trajectory analysis does not allow one to describe either the nonanalytical (singular) behavior of HHG rates near the thresholds of multiphoton ionization channels or the dependence of HHG rates on the parity of the multiphoton ionization channels and on the orbital angular momentum of the initial state (see Fig. 1).

The Baz' theory of threshold phenomena [69], which are observed in the cross sections of open multiphoton channel processes at the closing of the lowest open channel of a process, provides a good description of singular features in HHG rates [43,47,48]. According to Ref. [69], at the closing of the lowest open channel the behavior of the partial cross sections in other open channels is $\propto |E - E_{\rm th}|^{l_{\rm min}+1/2}$, where E is the energy of an open reaction channel, $E_{\rm th}$ is the threshold energy for the lowest channel, and $l_{\rm min}$ is the minimal allowed orbital angular momentum in the closing channel. The cusp- or steplike behaviors of cross sections as functions of the energy in open channels occur for $l_{\rm min} = 0$, while for $l_{\rm min} \geqslant 1$ the cross sections are smooth functions at $E = E_{\rm th}$.

The simplest case for our phenomenological analysis is that of an initial bound s state ($l = 0, m = 0$). According to dipole selection rules, the absorption of a linearly polarized photon changes the orbital angular momentum l by one ($l' = l \pm 1$) and keeps the magnetic projection unchanged if the polarization axis coincides with the quantization axis (otherwise the magnetic projection is changed by one, $m' = m \pm 1$). Thus the absorption of an odd (even) number of photons changes the orbital angular momentum of the active electron by an odd (even) number. For the two-color field, an even multiphoton ionization channel involves two partial channels. The first one corresponds to the absorption of an odd number of photons with energy $2\hbar\omega$ and an even number of photons with energy $\hbar\omega$. The second one corresponds to the absorption of an even number of photons with energy $2\hbar\omega$ and an even number of photons with energy $\hbar\omega$. The partial ionization channel with absorption of an odd number of photons with energy $2\hbar\omega$ may populate a continuum state with minimal orbital angular momentum $l_{\rm min} = 1$ (since the number of involved photons is odd), while the second partial channel may populate an ionization channel with $l_{\rm min} = 0$. Thus for an initial s state the cusp- or steplike behavior of

threshold phenomena should be observed at the closing of an even parity multiphoton ionization channel for both even and odd harmonics [see Figs. 1(a) and 1(b)]. The odd multiphoton ionization channel corresponds to absorption of an odd number of photons with energy $\hbar\omega$ and an arbitrary number of photons with energy $2\hbar\omega$. Since the components of a two-color field are linearly polarized in orthogonal directions, according to dipole selection rules, the interaction of the active electron with these components cannot lead to an ionization channel with $l = 0$ and thus the closing of an odd multiphoton ionization channel for an initial s-state results in a smoother ($\propto |E - E_{\rm th}|^{3/2}$) threshold behavior of the HHG rates.

For an initial p state, the cusp- or steplike threshold behavior of HHG rates is sensitive to both the parity of the harmonics and the parity of the closing multiphoton ionization channel (see Sec. III A). In order to explain this sensitivity, we note that the triply degenerate (in the magnetic projection quantum number) p state splits in a two-color field into three states, so that each of them has zero magnetic projection on one of the three Cartesian coordinate axes [38] [cf. Eqs. (A10) and (A11)]. The state with zero magnetic projection on the Z axis (ψ_0, $l = 1$, $m_z = 0$) does not contribute, since the laser-induced dipole is perpendicular to the orientation of this state. The state having zero magnetic projection on the X axis (ψ_-, $l = 1$, $m_x = 0$) contributes significantly to the generation of odd harmonics, while the state with zero magnetic projection on the Y axis (ψ_+, $l = 1$, $m_y = 0$) contributes to the generation of even harmonics [38]. Indeed, the generation of odd harmonics is controlled by the laser-induced dipole produced by the fundamental frequency component. Owing to the orthogonality relation ($\mathbf{e}_\omega \cdot \mathbf{e}_{2\omega}$) = 0, the dipole producing odd harmonics can be composed only from an odd number of vectors $\mathbf{e}_\omega$ and an even number of vectors $\mathbf{e}_{2\omega}$, thus having the form

$$\mathbf{d}_{2N+1} = \mathbf{e}_\omega d_{2N+1}, \tag{29}$$

where d_{2N+1} is a scalar independent of an even number of orthogonal vectors $\mathbf{e}_\omega$ and $\mathbf{e}_{2\omega}$, which fall out of the problem by forming scalar products ($\mathbf{e}_\omega \cdot \mathbf{e}_\omega$) = 1 and ($\mathbf{e}_{2\omega} \cdot \mathbf{e}_{2\omega}$) = 1. The direction of the dipole $\mathbf{d}_{2N+1}$ coincides with that of the X axis and thus the state with zero magnetic projection on the X axis should give the major contribution to the generation of odd harmonics. [According to Eq. (29), the odd harmonics are linearly polarized along the X axis [70].] Similarly, the dipole for even harmonics can only be composed from an odd number of vectors $\mathbf{e}_{2\omega}$ and an even number of vectors $\mathbf{e}_\omega$:

$$\mathbf{d}_{2N} = \mathbf{e}_{2\omega} d_{2N}, \tag{30}$$

where d_{2n} is a scalar independent of the vectors $\mathbf{e}_\omega$ and $\mathbf{e}_{2\omega}$. Thus the vector $\mathbf{d}_{2N}$ is directed along the Y axis and the state ψ_+ oriented along the Y axis contributes most to emission of linearly polarized (along the Y axis) even harmonics [70]. These phenomenological considerations and the general results (29) and (30) for HHG dipoles agree with analytic results of the TDER model presented in the Appendix. Moreover, since the results (29) and (30) for the directions of the HHG dipoles are valid for both threshold-enhanced and "regular" harmonics, the threshold phenomena we analyze do not affect the polarization properties of the harmonics.

The occurrence of threshold phenomena for an initial p state may be summarized as follows. According to dipole selection rules, if the active electron is in the ψ_- state ($l = 1$, $m_x = 0$), a multiphoton transition into a channel with zero magnetic projection ($m_x = 0$) is possible in general only if the electron absorbs an even number of photons with polarization vector $\mathbf{e}_{2\omega}$ (oriented along the Y axis) and any number of photons with polarization vector $\mathbf{e}_\omega$. For HHG, according to Eq. (29), the number of photons with polarization vector $\mathbf{e}_\omega$ should be odd. Finally, for an initial p state, a multiphoton ionization channel with $l = 0$ can be populated only if the number of absorbed photons is odd. As a result, the closing of an odd multiphoton ionization channel leads to cusp- or steplike behavior of the HHG rates for odd harmonics. Similar considerations show that for an active electron in a ψ_+ state ($l = 1$, $m_y = 0$), the absorption of an even number of $\hbar\omega$ photons and an odd number of $2\hbar\omega$ photons makes possible the population of a continuum channel with $l = 0$. Thus singularities in the HHG rates of even harmonics are observed at the closing of an even multiphoton ionization channel.

IV. SUMMARY

In this work we have studied threshold phenomena in HHG spectra produced by a two-color laser field, whose two components (with frequencies ω and 2ω) are linearly polarized in orthogonal directions. Our TDER analysis shows that in the case of a weak second harmonic component and an initial s state, the threshold anomalies (such as the cusp- or steplike behavior of HHG rates) are more pronounced near those thresholds of multiphoton ionization channels that correspond to even values of the channel-closing number R. Thus the threshold behavior of HHG rates for a two-color field and an initial s state is similar to that for the case of a linearly polarized single-component field [43,47]. However, for a p state we have found that even harmonics have singular cusp- or steplike behavior near those multiphoton ionization channels that correspond to even values of R, while for odd harmonics such singularities are observed at the closing of multiphoton ionization channels with odd channel-closing numbers (as for the case of a linearly polarized monochromatic field [47]). This sensitivity of the threshold behavior of HHG rates to the parity of multiphoton ionization channels is associated with the formation (from substates of the triply degenerate p state) of the two states, ψ_- and ψ_+, whose magnetic projections on the polarization vectors $\mathbf{e}_\omega$ and $\mathbf{e}_{2\omega}$ of the two-color field components are respectively equal to zero [cf. Eq. (A10)]. Based on dipole selection rules, we have shown that a two-color laser field can populate multiphoton ionization channels with zero orbital momentum of the ionized electron in alternative ways. For even harmonics this is realized in even

multiphoton ionization channels and for odd harmonics in odd channels. Thus, according to the general analysis of threshold phenomena [69], the closing of the corresponding channel leads to cusp- or steplike features in the intensity dependence of HHG rates.

In contrast to the case of a weak second harmonic component, for which the threshold singularities in HHG rates are not sensitive to the relative phase ϕ between the components of a two-color field, threshold anomalies for the case of comparable intensities of both components are highly sensitive to the relative phase. As our analysis shows, for the phase $\phi = \pi n$ (where n is an integer) the threshold phenomena are similar to those in HHG spectra for the case of a weak second harmonic component. However, for the phase $\phi = \pi/2 + \pi n$, the threshold phenomena in HHG spectra disappear, so that the intensity dependence of HHG rates in this case at the closing of multiphoton ionization channels is described by smooth curves [cf. Figs. 2(b) and 3(b)]. This suppression of threshold singularities in two-color HHG spectra as the relative phase changes from $\phi = \pi n$ to $\phi = \pi/2 + \pi n$ originates from a decreased number of quantum trajectories whose properties (times of ionization and recombination) are close to those for classically allowed closed trajectories in a single-component laser field. (The "closeness" of the quantum trajectories to the classical trajectories minimizes the imaginary part of the classical action along these trajectories and ensures a large number of contributing trajectories, whose interference at the multiphoton thresholds forms threshold singularities [45,46].) For the two-color field we have considered, the phase $\phi = n\pi$ ensures more favorable conditions, for which the quantum orbits are closer to the classical ones. In contrast, for $\phi = \pi/2 + \pi n$, there is only one trajectory contributing on each half-period of the two-color field; all others are suppressed due to the large imaginary part of the classical action, i.e., due to suppression of the ionization factors. Thus threshold peculiarities do not appear. Finally, we note that threshold phenomena in above-threshold ionization (ATI) in a two-color field are also modified as compared to the case of ATI in a single-frequency field. However, the specifics of threshold phenomena in such a two-color ATI process require a separate, detailed analysis.

ACKNOWLEDGMENTS

APPENDIX: TDER MODEL HHG AMPLITUDES AND RATES

In this Appendix we present the explicit form for the HHG dipole in the strong field approximation (SFA) for s and p states of a bound electron. Similar to the case of a monochromatic field, our calculations show that for a low-frequency two-color field ($\omega \ll |E_0|$), the SFA results in the TDER model are in good agreement with exact (numerically calculated) TDER results. Thus we present the corresponding HHG dipoles in the SFA. We emphasize that for any initial bound state the dipole for odd harmonics is defined by its X-axis projection, while the y projection of the HHG dipole is equal to zero. For even harmonics, the Y-axis component of the HHG dipole is nonzero, while the X-axis component is zero.

1. HHG amplitudes and rates for an initial s state

For an s state with energy $E_0 = -\kappa^2/2$, the HHG amplitude for odd harmonics ($\Omega = N\omega$, $N = 2n + 1$) for the two-color field (1) has the form

$$d_{2n+1}^{(x)} = \mathcal{N}_0 \int_0^\infty \frac{e^{i\lambda(\tau)}}{\tau^{3/2}} [j_-^{(1)}(\tau)\mathcal{C}_n(\tau;\phi) - ij_+^{(1)}(\tau)\mathcal{C}_{n+1}(\tau;\phi)]d\tau, \tag{A1}$$

while for even harmonics ($N = 2n + 2$) the result is

$$d_{2n+2}^{(y)} = \frac{\beta\mathcal{N}_0}{2} \int_0^\infty \frac{e^{i\lambda(\tau)}}{\tau^{3/2}} [e^{-i\phi} j_-^{(2)}(\tau)\mathcal{C}_n(\tau;\phi) + e^{i\phi} j_+^{(2)}(\tau)\mathcal{C}_{n+2}(\tau;\phi)]d\tau, \tag{A2}$$

where

$$\mathcal{N}_0 = i^{n+1/2}\frac{\kappa C_{\kappa 0} F}{4\Omega^2\sqrt{\pi\omega}}, \quad \epsilon = -\frac{\kappa^2}{2u_p} - 1, \tag{A3}$$

$$\lambda(\tau) = \frac{2u_p}{\omega}\left[\epsilon\tau + \frac{\sin^2(\tau)}{\tau} + \beta^2\frac{\sin^2(2\tau)}{16\tau}\right], \tag{A4}$$

$$j_\pm^{(s)} = \frac{\sin(s\tau)\sin(N\tau)}{s\tau} - \frac{N}{N\pm s}\sin[(N\pm s)\tau], \tag{A5}$$

$$\mathcal{C}_M(\tau;\phi) = \sum_{m=-\infty}^{\infty} i^{-m} J_{M-2m}(z_1)J_m\left(\frac{\beta^2}{8}z_2\right)e^{-2im\phi}, \quad u_p = \frac{F^2}{4\omega^2}, \tag{A6}$$

$$z_s = \frac{u_p}{\omega}\left[\sin(2s\tau) - 2\frac{\sin^2(s\tau)}{s\tau}\right], \tag{A7}$$

$J_k(z)$ is the Bessel function, and $C_{\kappa l}$ is the coefficient in the asymptotic form of the radial wave function $R_{\kappa l}(r)$ for the bound state of an electron with energy E_0 and angular momentum l in a short-range potential:

$$R_{\kappa l}(r \gg \kappa^{-1}) = C_{\kappa l}r^{-1}\exp(-\kappa r). \tag{A8}$$

The HHG rate for an s-state is given by the expression

$$\mathcal{R}_N = \frac{\Omega^3|\mathbf{d}_N|^2}{2\pi c^3}, \tag{A9}$$

where $\mathbf{d}_N = \mathbf{e}_\omega d_{2n+1}^{(x)}$ for odd harmonics and $\mathbf{d}_N = \mathbf{e}_{2\omega} d_{2n+2}^{(y)}$ for even harmonics.

2. HHG amplitudes and rates for an initial p state

In a two-color field with orthogonal linear polarizations, instead of the common description of a triply degenerate p state in terms of three substates with different projections of the orbital momentum on the Z axis ($m = 0$ and ± 1) it is convenient to introduce three other substates, which correspond to zero magnetic quantum numbers on the X (ψ_-), Y (ψ_+), and Z axes (ψ_0):

$$\psi_\pm(\mathbf{r}) = \varphi_{\kappa l}(r)[Y_{1,1}(\hat{\mathbf{r}}) \pm Y_{1,-1}(\hat{\mathbf{r}})], \tag{A10}$$

$$\psi_0(\mathbf{r}) = \varphi_{\kappa l}(r)Y_{1,0}(\hat{\mathbf{r}}), \tag{A11}$$

where $\varphi_{\kappa l}(r)$ is the radial wave function. Below we present only the HHG dipoles for the $\psi_\pm$ states, since the contribution of the ψ_0 state is negligibly small [since this state is "oriented" orthogonally to the field $\mathbf{F}(t)$]. Thus the total HHG rate $\mathcal{R}_N$ for a p state is given by a sum of partial rates for the states $\psi_\pm$:

$$\mathcal{R}_N = \tfrac{1}{3}(\mathcal{R}_N^{(-)} + \mathcal{R}_N^{(+)}), \tag{A12}$$

$$\mathcal{R}_N^{(\pm)} = \frac{\Omega^3|\mathbf{d}_N^{(\pm)}|^2}{2\pi c^3}. \tag{A13}$$

a. HHG amplitude for the ψ_+ state

For the case of odd harmonics: $N = 2n + 1$, $\mathbf{d}_N^{(+)} = \mathbf{e}_\omega d_{2n+1}^{(x)}$,

$$d_{2n+1}^{(x)} = \mathcal{N}_1 \int_0^\infty \frac{e^{i\lambda(\tau)}}{\tau^{3/2}}\left\{\frac{1}{2\tau}\left[j_-^{(1)}(\tau)\mathcal{C}_n(\tau;\phi) - ij_+^{(1)}(\tau)\mathcal{C}_{n+1}(\tau;\phi)\right] + \frac{u_p\beta^2}{2\omega}\left[ij_-^{(1)}(\tau)\Lambda_n^{(2)}(\tau;\phi) + j_+^{(1)}(\tau)\Lambda_{n+1}^{(2)}(\tau;\phi)\right]\right\}d\tau. \tag{A14}$$

For the case of even harmonics: $N = 2n + 2$, $\mathbf{d}_N^{(+)} = \mathbf{e}_{2\omega} d_{2n+2}^{(y)}$,

$$d_{2n+2}^{(y)} = \frac{\beta \mathcal{N}_1}{2} \int_0^\infty \frac{e^{i\lambda(\tau)}}{\tau^{3/2}} \left\{ \frac{1}{2\tau} [e^{-i\phi} j_-^{(2)}(\tau) \mathcal{C}_n(\tau;\phi) + e^{i\phi} j_+^{(2)}(\tau) \mathcal{C}_{n+2}(\tau;\phi)] \right.$$

$$\left. + i \frac{u_p \beta^2}{2\omega} [e^{-i\phi} j_-^{(2)}(\tau) \Lambda_n^{(2)}(\tau;\phi) + e^{i\phi} j_+^{(2)}(\tau) \Lambda_{n+2}^{(2)}(\tau;\phi)] + N [e^{-i\phi} v_-^{(2)} \mathcal{C}_n(\tau;\phi) + e^{i\phi} v_+^{(2)} \mathcal{C}_{n+2}(\tau;\phi)] \right\} d\tau, \quad \text{(A15)}$$

where

$$\mathcal{N}_1 = -i^{n+1/2} \frac{3 C_{\kappa 1} F}{4 \kappa \Omega^2} \sqrt{\frac{\omega}{\pi}}, \quad \text{(A16)}$$

$$\Lambda_q^{(s)}(\tau;\phi) = v_-^{(s)} \mathcal{C}_q(\tau;\phi) - \frac{1}{2} v_+^{(s)} i^s [e^{2i(s-1)\phi} \mathcal{C}_{q+s} + (-1)^s e^{-2i(s-1)\phi} \mathcal{C}_{q-s}], \quad \text{(A17)}$$

$$v_\pm^{(s)} = \left(\frac{\sin(s\tau)}{s\tau} - \cos(s\tau) \right) \left(\frac{\sin(N\tau)}{N\tau} - \cos(N\tau) \right) \pm \sin(N\tau) \sin(s\tau). \quad \text{(A18)}$$

b. HHG amplitude for the ψ_- state

For the case of odd harmonics: $N = 2n + 1$, $\mathbf{d}_N^{(-)} = \mathbf{e}_\omega d_{2n+1}^{(x)}$,

$$d_{2n+1}^{(x)} = \mathcal{N}_1 \int_0^\infty \frac{e^{i\lambda(\tau)}}{\tau^{3/2}} \left\{ \frac{1}{2\tau} [j_-^{(1)}(\tau) \mathcal{C}_n(\tau;\phi) - i j_+^{(1)}(\tau) \mathcal{C}_{n+1}(\tau;\phi)] + 2 \frac{u_p}{\omega} [i j_-^{(1)}(\tau) \Lambda_n^{(1)}(\tau;\phi) + j_+^{(1)}(\tau) \Lambda_{n+1}^{(1)}(\tau;\phi)] \right.$$

$$\left. + N [v_-^{(1)} \mathcal{C}_n(\tau;\phi) - i v_+^{(1)} \mathcal{C}_{n+1}(\tau;\phi)] \right\} d\tau. \quad \text{(A19)}$$

For the case of even harmonics: $N = 2n + 2$, $\mathbf{d}_N^{(-)} = \mathbf{e}_{2\omega} d_{2n+2}^{(x)}$,

$$d_{2n+2}^{(y)} = \frac{\beta \mathcal{N}_1}{2} \int_0^\infty \frac{e^{i\lambda(\tau)}}{\tau^{3/2}} \left\{ \frac{1}{2\tau} [e^{-i\phi} j_-^{(2)}(\tau) \mathcal{C}_n(\tau;\phi) + e^{i\phi} j_+^{(2)}(\tau) \mathcal{C}_{n+2}(\tau;\phi)] \right.$$

$$\left. + 2i \frac{u_p}{\omega} [e^{-i\phi} j_-^{(2)}(\tau) \Lambda_n^{(1)}(\tau;\phi) + e^{i\phi} j_+^{(2)}(\tau) \Lambda_{n+2}^{(1)}(\tau;\phi)] \right\} d\tau. \quad \text{(A20)}$$

[1] M.-C. Chen, P. Arpin, T. Popmintchev, M. Gerrity, B. Zhang, M. Seaberg, D. Popmintchev, M. M. Murnane, and H. C. Kapteyn, Bright, Coherent, Ultrafast Soft X-ray Harmonics Spanning the Water Window From a Tabletop Light Source, Phys. Rev. Lett. **105**, 173901 (2010).

[2] T. Popmintchev, M.-C. Chen, P. Arpin, M. M. Murnane, and H. C. Kapteyn, The attosecond nonlinear optics of bright coherent X-ray generation, Nat. Photon. **4**, 822 (2010).

[3] M.-C. Chen, C. Mancuso, C. Hernández-García, F. Dollar, B. Galloway, D. Popmintchev, P.-C. Huang, B. Walker, L. Plaja, A. A. Jaroń-Becker *et al.*, Generation of bright isolated attosecond soft x-ray pulses driven by multicycle midinfrared lasers, Proc. Natl. Acad. Sci. USA **111**, E2361 (2014).

[4] C. Hernandez-Garcia, T. Popmintchev, M. M. Murnane, H. C. Kapteyn, L. Plaja, A. A. Jaron-Becker, and A. Becker, Efficient generation of isolated attosecond soft x-ray pulses, in *Frontiers in Optics 2014, OSA Technical Digest (online)* (Optical Society of America, Washington, D.C., 2014), p. JTu5G.3.

[5] D. Shafir, H. Soifer, B. D. Bruner, M. Dagan, Y. Mairesse, S. Patchkovskii, M. Yu. Ivanov, O. Smirnova, and N. Dudovich, Resolving the time when an electron exits a tunneling barrier, Nature (London) **485**, 343 (2012).

[6] P. M. Kraus, B. Mignolet, D. Baykusheva, A. Rupenyan, L. Horný, E. F. Penka, G. Grassi, O. I. Tolstikhin, J. Schneider, F. Jensen, L. B. Madsen, A. D. Bandrauk, F. Remacle, and H. J. Wörner, Measurement and laser control of attosecond charge migration in ionized iodoacetylene, Science **350**, 790 (2015).

[7] D. Shafir, Y. Mairesse, D. M. Villeneuve, P. B. Corkum, and N. Dudovich, Atomic wavefunctions probed through strong-field light–matter interaction, Nat. Phys. **5**, 412 (2009).

[8] A. D. Shiner, B. E. Schmidt, C. Trallero-Herrero, H. J. Wörner, S. Patchkovskii, P. B. Corkum, J.-C. Kieffer, F. Légaré, and D. M. Villeneuve, Probing collective multi-electron dynamics in xenon with high-harmonic spectroscopy, Nat. Phys. **7**, 464 (2011).

[9] C Vozzi, M Negro, F Calegari, G Sansone, M Nisoli, S De Silvestri, and S Stagira, Generalized molecular orbital tomography, Nat. Phys. **7**, 822 (2011).

[10] P. B. Corkum, Plasma Perspective on Strong Field Multiphoton Ionization, Phys. Rev. Lett. **71**, 1994 (1993).

[11] P. B. Corkum and F. Krausz, Attosecond science, Nat. Phys. **3**, 381 (2007).

[12] M. Lewenstein, Ph. Balcou, M. Yu. Ivanov, A. L'Huillier, and P. B. Corkum, Theory of high-harmonic generation by low-frequency laser fields, Phys. Rev. A **49**, 2117 (1994).

[13] M. Yu. Ivanov, T. Brabec, and N. Burnett, Coulomb corrections and polarization effects in high-intensity high-harmonic emission, Phys. Rev. A **54**, 742 (1996).

[14] A. Baltuška, Th. Udem, M. Uiberacker, M. Hentschel, E. Goulielmakis, Ch. Gohle, R. Holzwarth, V. S. Yakovlev, A. Scrinzi, T. W. Hänsch, and F. Krausz, Attosecond control of electronic processes by intense light fields, Nature (London) **421**, 611 (2003).

[15] M. Nisoli, G. Sansone, S. Stagira, S. De Silvestri, C. Vozzi, M. Pascolini, L. Poletto, P. Villoresi, and G. Tondello, Effects of Carrier-envelope Phase Differences of Few-optical-cycle Light Pulses in Single-shot High-order-harmonic Spectra, Phys. Rev. Lett. **91**, 213905 (2003).

[16] M. V. Frolov, N. L. Manakov, A. M. Popov, O. V. Tikhonova, E. A. Volkova, A. A. Silaev, N. V. Vvedenskii, and A. F. Starace, Analytic Theory of High-order-harmonic Generation by an Intense Few-cycle Laser Pulse, Phys. Rev. A **85**, 033416 (2012).

[17] F. A. Weihe, S. K. Dutta, G. Korn, D. Du, P. H. Bucksbaum, and P. L. Shkolnikov, Polarization of high-intensity high-harmonic generation, Phys. Rev. A **51**, R3433 (1995).

[18] N. H. Burnett, C. Kan, and P. B. Corkum, Ellipticity and polarization effects in harmonic generation in ionizing neon, Phys. Rev. A **51**, R3418 (1995).

[19] P. Antoine, A. L'Huillier, M. Lewenstein, P. Salières, and B. Carré, Theory of high-order harmonic generation by an elliptically polarized laser field, Phys. Rev. A **53**, 1725 (1996).

[20] N. L. Manakov, Dissipation-induced effects in the generation of harmonics of a strong elliptically polarized light field in gases, Zh. Eksp. Teor. Fiz. **110**, 1244 (1996) [Sov. Phys. JETP **83**, 685 (1996)].

[21] B. Borca, A. V. Flegel, M. V. Frolov, N. L. Manakov, D. B. Milošević, and A. F. Starace, Static-electric-field-induced Polarization Effects in Harmonic Generation, Phys. Rev. Lett. **85**, 732 (2000).

[22] M. Möller, Y. Cheng, S. D. Khan, B. Zhao, K. Zhao, M. Chini, G. G. Paulus, and Z. Chang, Dependence of high-order-harmonic-generation yield on driving-laser ellipticity, Phys. Rev. A **86**, 011401(R) (2012).

[23] M. V. Frolov, N. L. Manakov, T. S. Sarantseva, and A. F. Starace, High-order-harmonic-generation spectroscopy with an elliptically polarized laser field, Phys. Rev. A **86**, 063406 (2012).

[24] I. J. Kim, C. M. Kim, H. T. Kim, G. H. Lee, Y. S. Lee, J. Y. Park, D. J. Cho, and C. H. Nam, Highly Efficient High-harmonic Generation in an Orthogonally Polarized Two-color Laser Field, Phys. Rev. Lett. **94**, 243901 (2005).

[25] C. M. Kim, I. J. Kim, and C. H. Nam, Generation of a strong attosecond pulse train with an orthogonally polarized two-color laser field, Phys. Rev. A **72**, 033817 (2005).

[26] C. M. Kim and C. H. Nam, Selection of an electron path of high-order harmonic generation in a two-colour femtosecond laser field, J. Phys. B **39**, 3199 (2006).

[27] Y. Zheng, Z. Zeng, P. Zou, L. Zhang, X. Li, P. Liu, R. Li, and Z. Xu, Dynamic Chirp Control and Pulse Compression for Attosecond High-order Harmonic Emission, Phys. Rev. Lett. **103**, 043904 (2009).

[28] L. Brugnera, D. J. Hoffmann, T. Siegel, F. Frank, A. Zaïr, J. W. G. Tisch, and J. P. Marangos, Trajectory Selection in High Harmonic Generation by Controlling the Phase Between Orthogonal Two-color Fields, Phys. Rev. Lett. **107**, 153902 (2011).

[29] C. Hutchison, S. Houver, N. Lin, D. J. Hoffmann, F. McGrath, T. Siegel, D. R. Austin, A. Zaïr, P. Salières, and J. P. Marangos, Electron trajectory control of odd and even order harmonics in high harmonic generation using an orthogonally polarised second harmonic field, J. Mod. Opt. **61**, 608 (2014).

[30] D. J. Hoffmann, C. Hutchison, A. Zaïr, and J. P. Marangos, Control of temporal mapping and harmonic intensity modulation using two-color orthogonally polarized fields, Phys. Rev. A **89**, 023423 (2014).

[31] Y. Zheng, H. Diao, Z. Zeng, X. Ge, R. Li, and Z. Xu, Manipulating electron-ion recollision in a midinfrared laser field, Phys. Rev. A **92**, 033417 (2015).

[32] D. Shafir, Y. Mairesse, H. J. Wörner, K. Rupnik, D. M. Villeneuve, P. B. Corkum, and N. Dudovich, Probing the symmetry of atomic wavefunctions from the point of view of strong field-driven electrons, New J. Phys. **12**, 073032 (2010).

[33] H. Niikura, N. Dudovich, D. M. Villeneuve, and P. B. Corkum, Mapping Molecular Orbital Symmetry on High-order Harmonic Generation Spectrum Using Two-color Laser Fields, Phys. Rev. Lett. **105**, 053003 (2010).

[34] H. Niikura, H. J. Wörner, D. M. Villeneuve, and P. B. Corkum, Probing the Spatial Structure of a Molecular Attosecond Electron Wave Packet Using Shaped Recollision Trajectories, Phys. Rev. Lett. **107**, 093004 (2011).

[35] L. Brugnera, F. Frank, D. J. Hoffmann, R. Torres, T. Siegel, J. G. Underwood, E. Springate, C. Froud, E. I. C. Turcu, J. W. G. Tisch, and J. P. Marangos, Enhancement of high harmonics generated by field steering of electrons in a two-color orthogonally polarized laser field, Opt. Lett. **35**, 3994 (2010).

[36] H. Soifer, M. Dagan, D. Shafir, B. D Bruner, M. Yu. Ivanov, V. Serbinenko, I. Barth, O. Smirnova, and N. Dudovich, Spatio-spectral analysis of ionization times in high-harmonic generation, Chem. Phys. **414**, 176 (2013).

[37] J. Zhao and M. Lein, Determination of Ionization and Tunneling Times in High-order Harmonic Generation, Phys. Rev. Lett. **111**, 043901 (2013).

[38] T. S. Sarantseva, M. V. Frolov, N. L. Manakov, M. Yu. Ivanov, and A. F. Starace, Harmonic generation spectroscopy with a two-colour laser field having orthogonal linear polarizations, J. Phys. B **46**, 231001 (2013).

[39] J. Cooper and R. N. Zare, in Photoelectron Angular Distributions, *Lectures in Theoretical Physics* Vol. XI-C, edited by S. Geltman, K. T. Mahanthappa, and W. E. Britten (Gordon and Breach, New York, 1969), pp. 317–337.

[40] M. Kitzler and M. Lezius, Spatial Control of Recollision Wave Packets with Attosecond Precision, Phys. Rev. Lett. **95**, 253001 (2005).

[41] J. Higuet, H. Ruf, N. Thiré, R. Cireasa, E. Constant, E. Cormier, D. Descamps, E. Mével, S. Petit, B. Pons, Y. Mairesse, and B. Fabre, High-order harmonic spectroscopy of the Cooper minimum in argon: Experimental and theoretical study, Phys. Rev. A **83**, 053401 (2011).

[42] P. Salières, B. Carré, L. Le Déroff, F. Grasbon, G. G. Paulus, H. Walther, R. Kopold, W. Becker, D. B. Milošević, A. Sanpera, and M. Lewenstein, Feynman's path-integral approach for intense-laser-atom interactions, Science **292**, 902 (2001).

[43] B. Borca, A. F. Starace, A. V. Flegel, M. V. Frolov, and N. L. Manakov, Threshold-related effects in high-order harmonic generation, Phys. Rev. A **65**, 051402(R) (2002).

[44] R. Kopold, W. Becker, M. Kleber, and G. G. Paulus, Channel-closing effects in high-order above-threshold ionization and high-order harmonic generation, J. Phys. B **35**, 217 (2002).

[45] S. V. Popruzhenko, Ph. A. Korneev, S. P. Goreslavski, and W. Becker, Laser-induced Recollision Phenomena: Interference Resonances at Channel Closings, Phys. Rev. Lett. **89**, 023001 (2002).

[46] D. B. Milošević and W. Becker, Role of long quantum orbits in high-order harmonic generation, Phys. Rev. A **66**, 063417 (2002).

[47] N. L. Manakov and M. V. Frolov, Threshold phenomena in the cross sections for atomic photoprocesses in a strong laser field, Pis'ma Zh. Eksp. Teor. Fiz. **83**, 630 (2006) [JETP Lett. **83**, 536 (2006)] .

[48] M. V. Frolov, N. L. Manakov, and A. F. Starace, Wavelength Scaling of High-harmonic Yield: Threshold Phenomena and Bound State Symmetry Dependence, Phys. Rev. Lett. **100**, 173001 (2008).

[49] K. Schiessl, K. L. Ishikawa, E. Persson, and J. Burgdörfer, Quantum Path Interference in the Wavelength Dependence of High-harmonic Generation, Phys. Rev. Lett. **99**, 253903 (2007).

[50] K. Schiessl, K. L. Ishikawa, E. Persson, and J. Burgdörfer, Wavelength dependence of high-harmonic generation from ultrashort pulses, J. Mod. Opt. **55**, 2617 (2008).

[51] K. L. Ishikawa, K. Schiessl, E. Persson, and J. Burgdörfer, Fine-scale oscillations in the wavelength and intensity dependence of high-order harmonic generation: Connection with channel closings, Phys. Rev. A **79**, 033411 (2009).

[52] M. V. Frolov, N. L. Manakov, E. A. Pronin, and A. F. Starace, Model-independent Quantum Approach for Intense Laser Detachment of a Weakly Bound Electron, Phys. Rev. Lett. **91**, 053003 (2003).

[53] M. V. Frolov, N. L. Manakov, and A. F. Starace, Effective-range theory for an electron in a short-range potential and a laser field, Phys. Rev. A **78**, 063418 (2008).

[54] M. V. Frolov, A. V. Flegel, N. L. Manakov, and A. F. Starace, Description of harmonic generation in terms of the complex quasienergy. II. Application to time-dependent effective range theory, Phys. Rev. A **75**, 063408 (2007).

[55] M. V. Frolov, N. L. Manakov, A. A. Silaev, and N. V. Vvedenskii, Analytic description of high-order harmonic generation by atoms in a two-color laser field, Phys. Rev. A **81**, 063407 (2010).

[56] N. L. Manakov and L. P. Rapoport, Particle with low binding energy in a circularly polarized field, Zh. Eksp. Teor. Fiz. **69**, 842 (1975) [Sov. Phys. JETP **42**, 430 (1976)].

[57] N. L. Manakov, V. D. Ovsiannikov, and L. P. Rapoport, Atoms in a laser field, Phys. Rep. **141**, 320 (1986).

[58] N. L. Manakov, M. V. Frolov, A. F. Starace, and I. I. Fabrikant, Interaction of laser radiation with a negative ion in the presence of a strong static electric field, J. Phys. B **33**, R141 (2000).

[59] S.-I. Chu and D. A. Telnov, Beyond the Floquet theorem: generalized Floquet formalisms and quasienergy methods for atomic and molecular multiphoton processes in intense laser fields, Phys. Rep. **390**, 1 (2004).

[60] L. D. Landau and E. M. Lifshitz, *Quantum Mechanics (Non-relativistic Theory)* (Pergamon Press, Oxford, 1977).

[61] M. V. Frolov, N. L. Manakov, T. S. Sarantseva, and A. F. Starace, Analytic confirmation that the factorized formula for harmonic generation involves the exact photorecombination cross section, Phys. Rev. A **83**, 043416 (2011).

[62] M. V. Frolov, A. V. Flegel, N. L. Manakov, and A. F. Starace, Description of harmonic generation in terms of the complex quasienergy. I. General formulation, Phys. Rev. A **75**, 063407 (2007).

[63] N. L. Manakov, M. V. Frolov, B. Borca, and A. F. Starace, Stabilization of bound state decay in an intense monochromatic high-frequency field, Pis'ma Zh. Eksp. Teor. Fiz. **72**, 426 (2000) [JETP Lett. **72**, 294 (2000)].

[64] N. L. Manakov, M. V. Frolov, B. Borca, and A. F. Starace, Multiphoton detachment of a negative ion by an elliptically polarized, monochromatic laser field, J. Phys. B **36**, R49 (2003).

[65] A. Gordon, R. Santra, and F. X. Kärtner, Role of the Coulomb singularity in high-order harmonic generation, Phys. Rev. A **72**, 063411 (2005).

[66] A. A. Silaev and N. V. Vvedenskii, Residual-current Excitation in Plasmas Produced by Few-cycle Laser Pulses, Phys. Rev. Lett. **102**, 115005 (2009).

[67] M. V. Frolov, N. L. Manakov, W.-H. Xiong, L.-Y. Peng, J. Burgdörfer, and A. F. Starace, Scaling laws for high-order harmonic generation with midinfrared laser pulses, Phys. Rev. A **92**, 023409 (2015).

[68] R. P. Feynman and A. R. Hibbs, *Quantum Mechanics and Path Integrals* (McGraw-Hill, New York, 1965).

[69] A. I. Baz', The energy dependence of a scattering cross section near the threshold of a reaction, Zh. Eksp. Teor. Fiz. **33**, 923 (1957) [Sov. Phys. JETP **6**, 709 (1958)].

[70] S. Long, W. Becker, and J. K. McIver, Model calculations of polarization-dependent two-color high-harmonic generation, Phys. Rev. A **52**, 2262 (1995).